RESEARCH ARTICLE | JULY 31 2024

Accurate recognition of light beams carrying orbital angular momentum through scattering media using ghost diffraction

Yonggui Cao ; Wen Chen

Appl. Phys. Lett. 125, 051107 (2024)
https://doi.org/10.1063/5.0220504

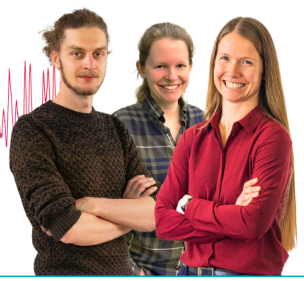

Applied Physics Letters ARTICLE pubs.aip.org/aip/apl

Accurate recognition of light beams carrying orbital angular momentum through scattering media using ghost diffraction

Cite as: Appl. Phys. Lett. **125**, 051107 (2024); doi: 10.1063/5.0220504
Submitted: 26 May 2024 · Accepted: 21 July 2024 ·
Published Online: 31 July 2024

Yonggui Cao[1] and Wen Chen[1,2,a)]

AFFILIATIONS

[1]Department of Electrical and Electronic Engineering, The Hong Kong Polytechnic University, Hong Kong, China
[2]Photonics Research Institute, The Hong Kong Polytechnic University, Hong Kong, China

[a)]Author to whom correspondence should be addressed: owen.chen@polyu.edu.hk

ABSTRACT

We report a ghost diffraction-based approach to realize accurate recognition of light beams carrying orbital angular momentum (OAM) through dynamic and complex scattering media. A bit sequence is first encoded into an OAM beam, which is sequentially modulated by a series of Hadamard patterns, and then an optical wave propagates through dynamic and complex scattering media. The collected single-pixel light intensities are temporally corrected, and ghost images can be reconstructed by using the principle of ghost diffraction. The reconstructed ghost images are further processed by using block-matching and 3D filtering with image registration, which are then utilized for OAM recognition assisted by the featured normalized cross correlation. Optical experiments are conducted to demonstrate that light beams carrying OAM can be accurately recognized in dynamic and complex scattering environments, and the proposed approach is feasible and effective. The developed ghost diffraction-based approach could open an avenue for various OAM-encoded applications in dynamic and complex scattering environments.

Orbital angular momentum (OAM)[1,2] is one of two forms of angular momentum of light and attracts much attention. An additional degree of freedom exists in OAM by exploiting the helical phase front of light beams. The helical phase structure imparts a quantized amount of angular momentum to the photons, allowing them to carry energy and OAM.[2] The interest of such states can be observed in various areas,[3–7] e.g., metrology,[4] communication,[6,7] etc. Although OAM was widely investigated, there is still concern about its recognition in scattering environments. In terms of OAM-encoded optical transmission through scattering media, it could be a challenge to extract OAM from the received signals. In addition, the classification is pivotal for effectively harnessing the full potential of OAM-encoded optical systems, and the precise manipulation and control of OAM modes need to be enabled. Some approaches were studied and applied for OAM recognition,[8–12] e.g., interference.[9,10] Deep learning[13–18] has also made significant strides in beam recognition. However, deep networks could require extensive training beforehand, and the parameters of deep learning could lack portability across different scenarios.[13] When light beams carrying OAM propagate through dynamic and complex scattering media, strong turbulence could affect the wavefront, which makes conventional receivers incapable of capturing effective data. Therefore, there is a need to further develop OAM recognition methods in order to address the challenge. It is widely recognized that ghost diffraction[19] can be studied to realize high-quality information retrieval in scattering environments. A temporal correction strategy[20,21] was also developed to enable high-resolution ghost retrieval.

Inspired by ghost diffraction principles, we realize the recognition of light beams carrying OAM through scattering media. Here, we report a ghost diffraction-based approach to realize the accurate recognition of light beams carrying OAM through dynamic and complex scattering media. The bit sequences are first encoded by using a combination of pre-selected OAM bases. The principle of ghost diffraction with a temporal correction is introduced for optical transmission in dynamic and complex scattering environments, and Hadamard patterns are utilized to sequentially modulate the OAM beam. A series of single-pixel light intensities are sequentially collected at the receiving end to be temporally corrected to recover a ghost image with an inverse Hadamard transform. The reconstructed ghost image is further processed by block-matching and 3D filtering (BM3D)[22] with image registration,[23] which is then utilized for OAM recognition assisted by

the featured normalized cross correlation (FNCC). Experimental results demonstrate that the proposed ghost diffraction-based approach can realize ultrahigh-accuracy OAM recognition and is robust against high scattering in the optical channel.

Light beams carrying OAM can be described by using Laguerre–Gaussian (LG) modes.[1,13] The LG beam can be described by

$$LG|p,l\rangle = I(t)\frac{\omega_0}{\omega(z)}e^{-\frac{r^2}{\omega(z)^2}}e^{-i\frac{2\pi}{\lambda}\frac{r^2 z}{2(z^2+R^2)}}e^{-i\frac{2\pi}{\lambda}z}\sqrt{\frac{2p!}{\pi\omega_0^2(p+|l|)!}}\left(\frac{\sqrt{2}r}{\omega(z)}\right)^{|l|} \times L_p^{|l|}\left(\frac{2r^2}{\omega(z)^2}\right)e^{-i(2p+|l|+1)\arctan\frac{z}{R}+il\theta}, \quad (1)$$

where (r,θ,z) denotes a cylindrical coordinate, $i=\sqrt{-1}$, ω_0 denotes the beam waist radius at the source, $I(t)$ denotes the initial intensity (usually be set to 1), R denotes the Rayleigh range, p denotes the order of the Laguerre polynomial, l denotes the topological charge of the beam carrying OAM, $L_p^{|l|}$ denotes an associated Laguerre polynomial, $\omega(z)$ denotes the radius of the beam at a distance z, and λ denotes the wavelength.

An OAM-encoded transmission scheme is presented to verify the proposed approach. In Fig. 1, three OAM bases ($LG|0,1\rangle$, $LG|0,-3\rangle$, and $LG|0,-4\rangle$) are pre-selected to be demonstrated as a typical example. A mapping relationship between bit sequences and OAM is established in Table I. For instance, bit sequence 010 means that phase and amplitude distributions of the OAM beam are generated by $0\times LG|0,1\rangle + 1\times LG|0,-3\rangle + 0\times LG|0,-4\rangle$. Since three bases are used, there are eight class labels. A look-up table is obtained to establish a mapping between bit sequence and the OAM. A flow chart for the proposed ghost diffraction-based approach is given in Fig. 2. Bit sequences are first encoded into OAM beams, and a series of phase masks containing phase information of OAM are generated and placed in an optical channel to modulate optical wave. Then, the light beam carrying OAM propagates in a designed Hadamard-based setup through dynamic and complex scattering media. At the receiving end, a ghost image is first recovered via a temporal correction[20,21] of the recorded single-pixel light intensities followed by an inverse

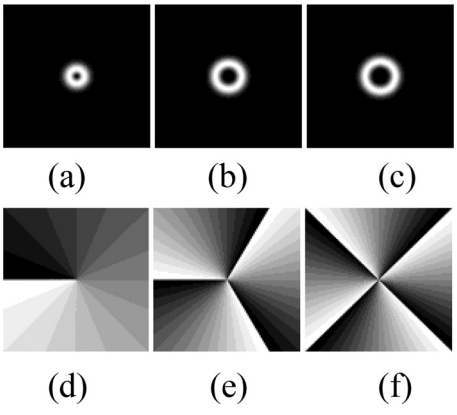

FIG. 1. Three OAM bases pre-selected for the designed OAM-encoded optical system: (a) and (d) intensity and phase patterns of $LG|0,1\rangle$; (b) and (e) intensity and phase patterns of $LG|0,-3\rangle$; and (c) and (f) intensity and phase patterns of $LG|0,-4\rangle$.

TABLE I. A mapping relationship among class label, bit sequence, and OAM intensity. In the established database, the generated intensity pattern for bit sequence 000 is re-set as all ones rather than all zeros for the calculation of NCC.

Class label	Bit sequence	Intensity	Class label	Bit sequence	Intensity
1	000		5	100	
2	001		6	101	
3	010		7	110	
4	011		8	111	

Hadamard transform, and then processed using BM3D[22] with image registration[23] aimed at correcting rotation and scale. The image registration process[23] is designed to align the coordinates of the recovered image with those in the database. These transformations are essential to achieve the precise alignment and ensure that the recovered ghost images can be accurately compared and analyzed. Finally, the normalized cross correlation (NCC) $\gamma(u,v)$ can be calculated by[24]

$$\gamma(u,v) = \frac{\sum_{x,y}\left[f(x,y)-\bar{f}_{u,v}\right]\left[h(x-u,y-v)-\bar{h}\right]}{\sqrt{\sum_{x,y}\left[f(x,y)-\bar{f}_{u,v}\right]^2\sum_{x,y}\left[h(x-u,y-v)-\bar{h}\right]^2}}, \quad (2)$$

where $f(x,y)$ denotes a ghost image obtained after image registration, $h(x,y)$ denotes an intensity pattern in Table I, $\bar{f}_{u,v}$ denotes the mean of $f(x,y)$ in the region under the intensity pattern in Table I, and $\bar{h}$ denotes the mean of the intensity pattern in Table I. Here, the maximum value of $\gamma(u,v)$ is defined as FNCC. Therefore, eight FNCC values need to be calculated when one bit sequence is transmitted. Through a comparison among the calculated FNCC values, an intensity pattern in Table I can be recognized so that the transmitted bit sequence can be retrieved accordingly.

An experimental setup for the proposed optical system was designed and is shown in Fig. 3. A laser (MGL-III-532, 200.0 mW) with a wavelength of 532.0 nm is collimated. An optical wave propagates through a zero-order half-wave plate (Thorlabs, WPHSM05-266) and then illuminates a phase-only spatial light modulator (SLM-1, Holoeye PLUTO2) with a pixel size of 8.0 μm. The phase mask embedded into SLM-1 is generated by combining the phase information of OAM and a grating.[25] The first diffraction order can be selected with an Iris. 16384 Hadamard patterns are sequentially embedded into an amplitude-only SLM (SLM-2, CASMICROSTAR FSLM-2K39-A02) with a pixel size of 4.5 μm, and a pre-generated random amplitude-only pattern is used before each Hadamard pattern. Then, an optical wave propagates through dynamic and complex

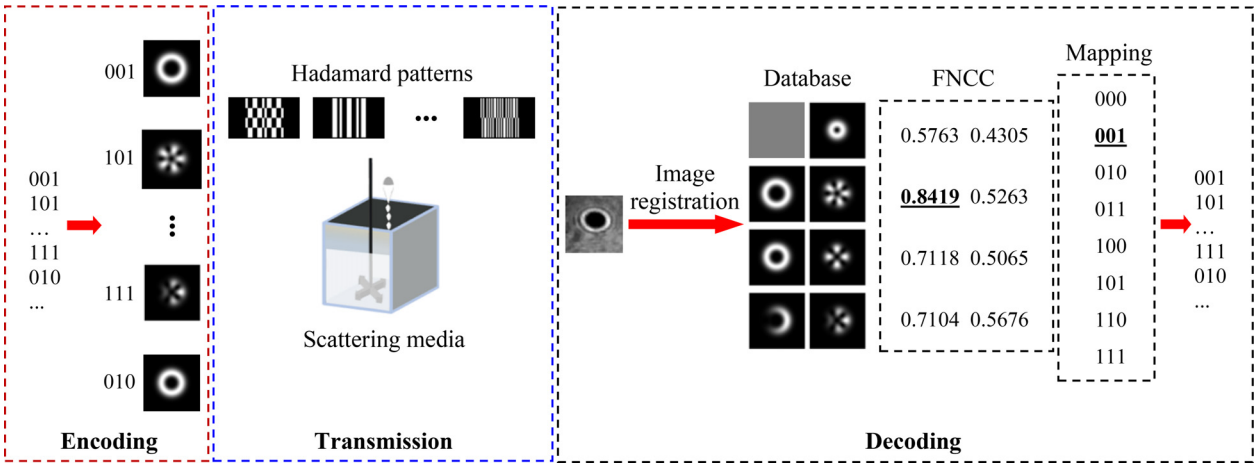

FIG. 2. A flow chart for the developed ghost diffraction-based method to realize an accurate recognition of light beams carrying OAM in dynamic and complex scattering environments. In the established database, the generated intensity pattern for bit sequence 000 is re-set as all ones rather than all zeros for the calculation of NCC in this study.

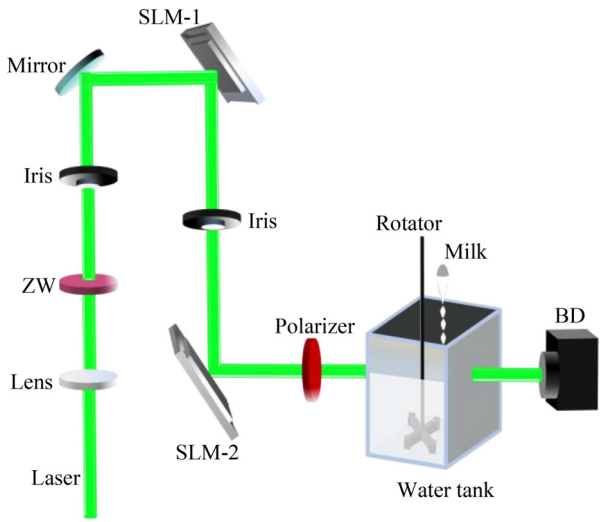

FIG. 3. A schematic experimental setup for the designed optical system. ZW: zero-order wave plate; BD: single-pixel bucket detector; SLM-1: phase-only spatial light modulator; SLM-2: amplitude-only spatial light modulator. The proposed method in other scattering media (e.g., with other physical parameters) can also be feasible.

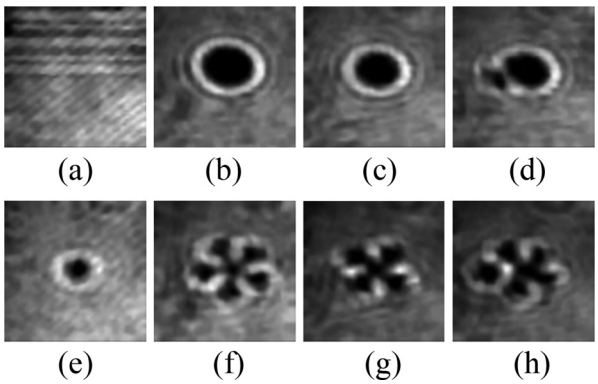

FIG. 4. Typical experimental results: (a)–(h) the recovered ghost images (obtained after the BM3D operation), respectively, corresponding to those in Table I, i.e., 000, 001, 010, 011, 100, 101, 110, and 111.

scattering media, and a water tank with $15.0 \times 10.0 \times 30.0\,\text{cm}^3$ (length × width × height) is used, which contains 3000.0 ml clean water. A rotator is kept operating at 700.0 rpm to create a dynamic environment, and 20.0 ml full-cream milk mixed with 500.0 ml clean water is continuously dropped into the water tank during the experiments. The axial distance between SLM-1 and SLM-2 is 60.0 cm. The axial distance between SLM-2 and the front side of the water tank is 15.0 cm, and the axial distance between the back side of the water tank and a single-pixel bucket detector is 5.0 cm. A single-pixel bucket detector without spatial resolution (Thorlabs, PDA100A2) is placed at the receiving end to collect single-pixel light intensities. The collected single-pixel light intensities can be temporally corrected,[20,21,26,27] since a fixed and random amplitude-only pattern has been applied in optical experiments.

As can be seen in Fig. 4, eight ghost images can be individually recovered in dynamic and complex scattering environments. The pattern in Fig. 4(a) can be considered a recovery of a Gaussian beam since no phase information related to OAM is used in the optical channel. The recovered ghost images in Figs. 4(b)–4(h) correspond to those intensity patterns in Table I, respectively.

The calculated FNCC values corresponding to those in Figs. 4(a)–4(h) are shown in Figs. 5(a)–5(d). For each recovered ghost image, eight FNCC values are calculated and then a bit sequence corresponding to the maximum FNCC value can be determined. For instance, as can be seen in the black curve of Fig. 5(a), the maximum FNCC value corresponds to class label 1. Therefore, the recovered ghost image in Fig. 4(a) is recognized, and its corresponding bit sequence is 000. It has been experimentally demonstrated that the ghost diffraction-based approach can realize accurate recognition of light beams carrying OAM through dynamic and complex scattering

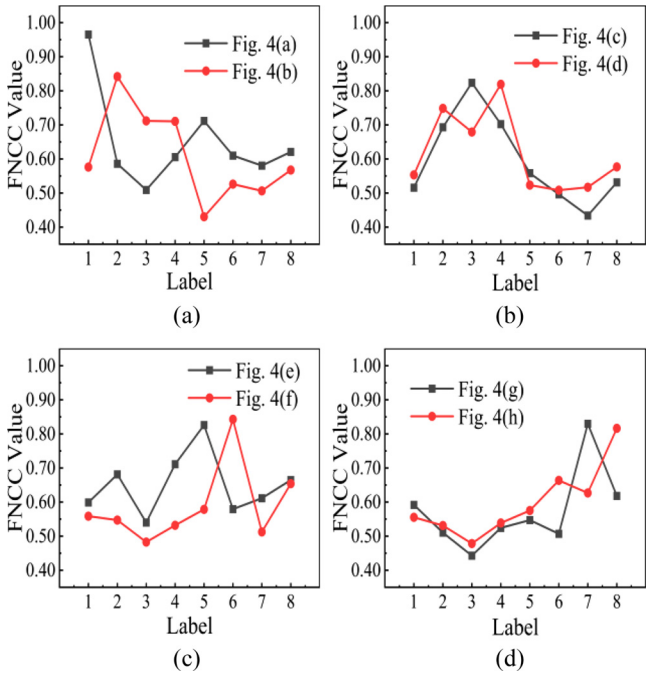

FIG. 5. (a)–(d) The FNCC, respectively, corresponding to Figs. 4(a)–4(h).

FIG. 6. A confusion matrix.

media. To further evaluate the accuracy and reliability, a series of optical experiments are conducted. 80 ghost images are recovered, and each bit sequence is encoded and tested 10 times. A confusion matrix is obtained and given in Fig. 6. The diagonal elements indicate ultrahigh-accuracy recognition achieved by using the proposed method based on ghost diffraction through dynamic and complex scattering media. It is worth noting that it could also be straightforward to encode and recognize a sequence with more bits using the proposed approach, and other OAM bases can also be pre-selected and applied.

In conclusion, we have reported a ghost diffraction-based approach to realize accurate recognition of light beams carrying OAM through dynamic and complex scattering media. The principle of ghost diffraction has been introduced to recover ghost images in dynamic and complex scattering environments for OAM transmission, and ultrahigh-accuracy recognition of OAM is realized. A series of optical experiments are conducted to illustrate the feasibility and effectiveness of the proposed approach, and the developed ghost diffraction-based approach could open an avenue for various OAM-encoded applications in dynamic and complex scattering environments.

This work was supported by the Hong Kong Research Grants Council (15223522 and 15224921), the GuangDong Basic and Applied Basic Research Foundation (2022A1515011858) and The Hong Kong Polytechnic University (1-BD4Q, 1-WZ4M).

AUTHOR DECLARATIONS

Conflict of Interest

The authors have no conflicts to disclose.

Author Contributions

Yonggui Cao: Investigation (lead); Writing – original draft (lead). **Wen Chen:** Conceptualization (lead); Investigation (lead); Methodology (lead); Supervision (lead); Writing – review & editing (lead).

DATA AVAILABILITY

The data that support the findings of this study are available from the corresponding author upon reasonable request.

REFERENCES

[1]L. Allen, M. W. Beijersbergen, R. Spreeuw, and J. Woerdman, Phys. Rev. A **45**, 8185 (1992).
[2]M. Padgett, J. Courtial, and L. Allen, Phys. Today **57**(5), 35 (2004).
[3]F. Cardano and L. Marrucci, Nat. Photon **9**, 776 (2015).
[4]H. Rubinsztein-Dunlop, A. Forbes, M. V. Berry, M. R. Dennis, D. L. Andrews, M. Mansuripur, C. Denz, C. Alpmann, P. Banzer, T. Bauer, E. Karimi, L. Marrucci, M. Padgett, M. Ritsch-Marte, N. M. Litchinitser, N. P. Bigelow, C. Rosales-Guzmán, A. Belmonte, J. P. Torres, T. W. Neely, M. Baker, R. Gordon, A. B. Stilgoe, J. Romero, A. G. White, R. Fickler, A. E. Willner, G. D. Xie, B. McMorran, and A. M. Weiner, J. Opt. **19**, 013001 (2016).
[5]X. Fang, H. Ren, and M. Gu, Nat. Photon. **14**, 102 (2020).
[6]T. Lei, M. Zhang, Y. Li, P. Jia, G. N. Liu, X. Xu, Z. Li, C. Min, J. Lin, and C. Yu, Light **4**, e257 (2015).
[7]J. Wang, J. Liu, S. Li, Y. Zhao, J. Du, and L. Zhu, Nanophotonics **11**, 645 (2022).
[8]J. Leach, M. J. Padgett, S. M. Barnett, S. Franke-Arnold, and J. Courtial, Phys. Rev. Lett. **88**, 257901 (2002).
[9]S. Slussarenko, V. D'Ambrosio, B. Piccirillo, L. Marrucci, and E. Santamato, Opt. Express **18**, 27205 (2010).
[10]H. Huang, Y. Ren, Y. Yan, N. Ahmed, Y. Yue, A. Bozovich, B. I. Erkmen, K. Birnbaum, S. Dolinar, M. Tur, and A. E. Willner, Opt. Lett. **38**, 2348 (2013).
[11]G. C. Berkhout, M. P. Lavery, J. Courtial, M. W. Beijersbergen, and M. J. Padgett, Phys. Rev. Lett. **105**, 153601 (2010).
[12]M. Malik, M. Mirhosseini, M. P. Lavery, J. Leach, M. J. Padgett, and R. W. Boyd, Nat. Commun. **5**, 3115 (2014).
[13]S. Avramov-Zamurovic, J. M. Esposito, and C. Nelson, J. Opt. Soc. Am. A **40**, 64 (2023).

[14]T. Giordani, A. Suprano, E. Polino, F. Acanfora, L. Innocenti, A. Ferraro, M. Paternostro, N. Spagnolo, and F. Sciarrino, Phys. Rev. Lett. **124**, 160401 (2020).
[15]Z. Liu, S. Yan, H. Liu, and X. Chen, Phys. Rev. Lett. **123**, 183902 (2019).
[16]M. I. Dedo, Z. Wang, K. Guo, and Z. Guo, Opt. Commun. **456**, 124696 (2020).
[17]F. Feng, J. Hu, Z. Guo, J.-A. Gan, P. F. Chen, G. Chen, C. Min, X. Yuan, and M. Somekh, ACS Photon. **9**, 820 (2022).
[18]J. J. Sun, S. Sun, and L. J. Yang, IEEE Trans. Antennas Propag. **70**, 6775–6784 (2022).
[19]R. S. Bennink, S. J. Bentley, and R. W. Boyd, Phys. Rev. Lett. **89**, 113601 (2002).
[20]Y. Cao, Y. Xiao, and W. Chen, Opt. Lett. **48**, 3491 (2023).
[21]Y. Xiao, L. Zhou, and W. Chen, Opt. Lett. **47**, 3692 (2022).
[22]K. Dabov, A. Foi, V. Katkovnik, and K. Egiazarian, IEEE Trans. Image Process. **16**, 2080 (2007).
[23]A. Myronenko and X. Song, IEEE Trans. Med. Imaging **29**, 1882 (2010).
[24]J. C. Yoo and T. Han, Circuits Syst. Signal Process. **28**, 819–843 (2009).
[25]L. Stoyanov, S. Topuzoski, I. Stefanov, L. Janicijevic, and A. Dreischuh, Opt. Commun. **350**, 301 (2015).
[26]Y. Xiao, L. Zhou, and W. Chen, Opt. Lasers Eng. **174**, 107957 (2024).
[27]Y. Peng and W. Chen, Opt. Lett. **48**, 4480 (2023).